# Role of *k*-point sampling in the supercell approach to inelastic electron tunneling spectroscopy simulations of molecular monolayers

Giuseppe Foti,[1,2,*] Daniel Sánchez-Portal,[1,2] Andrés Arnau,[1,2,3] and Thomas Frederiksen[2,4]

[1]*Centro de Física de Materiales, Centro Mixto CSIC-UPV, Paseo Manuel de Lardizabal 5, Donostia-San Sebastián, Spain*

[2]*Donostia International Physics Center (DIPC), Paseo Manuel de Lardizabal 4, Donostia-San Sebastián, Spain*

[3]*Departmento de Física de Materiales UPV/EHU, Facultad de Química, Apdo. 1072, Donostia-San Sebastián, Spain*

[4]*IKERBASQUE, Basque Foundation for Science, E-48013 Bilbao, Spain*

(Received 14 February 2014; revised manuscript received 12 December 2014; published 23 January 2015)

While the role of sampling of the electron momentum $k$ in supercell calculations of the elastic electron transmission is well understood, its influence in the case of inelastic electron tunneling (IET) has not yet been systematically explored. Here we compare *ab initio* IET spectra of molecular monolayers in the commonly used Γ-point approximation to rigorously $k$-converged results. We study four idealized molecular junctions with either alkanedithiolates or benzenedithiolates, and explore variations due to varying molecular tilt angle, density, as well as chemical identity of the monolayer. We show that the Γ-point approximation is reasonable for a range of systems, but that a rigorous convergence is needed for accurate signal amplitudes. We also describe an approximative scheme which reduces the computational cost of the $k$-averaged calculation in our implementation.

DOI: 10.1103/PhysRevB.91.035434 PACS number(s): 73.63.−b, 72.10.Di, 71.15.Mb

## I. INTRODUCTION

Inelastic electron tunneling spectroscopy (IETS) is a powerful method to characterize molecular junctions since it gives the vibrational fingerprint of molecular adsorbates and allows us to access the conformational degree of freedom of nanostructures and their chemical composition [1–3]. At low temperatures the vibrational motion of molecules is almost completely frozen. However, when electronic currents pass through the junction, molecular vibrations can be excited by the electrons (if they have enough energy). These effects appear as nonlinearities in the current-voltage ($I$-$V$) characteristics of the junction.

First-principles IETS calculations based on density functional theory (DFT) in combination with nonequilibrium Green's functions (NEGF) is now a well-established technique [4–14] but it has traditionally been used in combination with the Γ-point approximation where all quantities (such as Green's functions and the electron-phonon coupling matrix) are calculated for $k = q = 0$, where $k$ and $q$ are the electron and phonon momenta, respectively [15]. For very large supercells this approximation tends to the exact solution since electron and phonon bands fold back to Γ. Nevertheless, in real calculations the supercell size is finite and convergence with respect to $k$ and $q$ is an open question. A periodic arrangement of molecules such as self-assembled monolayers (SAM) thus represent a critical testbed for the traditional approach.

Alkanedithiolates (ADT) represent a prototype tunnel junction [16–20] and their IETS spectra are among the best characterized [21–31]. From a theoretical point of view they thus provide a good reference for testing new computational strategies. Here we calculate first-principles IETS spectra of SAMs formed by ADT in a dense and dilute monolayer and with two different tilt angles with respect to surface normal. Increasing the tilt angle of the ADT affects the band alignment process [32] and may introduce intermolecular tunneling pathways for current, resulting in an enhancement of the conductance at the Fermi level [33,34]. We also explore resonant transport conditions as exemplified by a SAM of benzenedithiolates (BDT), another molecular species that has been studied extensively [35–40]. Based on our comparison of the $k$ convergence of the IETS spectra in these different situations, we find that the Γ-point approximation is a fair approximation for a qualitative description of the considered systems, but that a rigorous $k$ sampling is needed for quantitative IETS signal amplitudes. Our findings suggest that when the e-ph couplings can be considered "local" with respect to a molecular transport pathway, the role of the initial electron phase in the bulk electrode is suppressed and the inelastic electron scattering cross section becomes essentially $k$ independent. We also present a simplified scheme to reduce the computational cost of our IETS calculations, in which the $k$ sampling is performed without considering explicitly the $k$ dependence in the e-ph couplings.

The paper is organized as follows: In Sec. II we give a theoretical description of the approximations used and introduce the computational details of our DFT calculations. The computed results for the elastic transmission and the IETS for the different SAMs are presented in Sec. III. Finally, in Sec. IV our conclusions are presented.

## II. METHODS

### A. Theory

DFT calculations in solid state physics typically rely on a supercell representation where the real system, which could be too large to be treated explicitly at an atomistic level, is approximated using a periodic system built up from a relatively small unit cell. Bloch's theorem gives the mathematical foundation of this approach. As a consequence, physical quantities such as the density of states (DOS) involve integrations over the first Brillouin zone (BZ) in reciprocal space. For an open quantum system, in which a scattering region is coupled to semi-infinite electrodes, periodicity in

*giuseppe_foti@ehu.es

 

the direction of the current is broken and the current $I$ is calculated as an average over the bidimensional BZ in the plane perpendicular to transport:

$$I(V) = \frac{1}{\Omega}\int_{\mathrm{BZ}} dk\, I(V,k), \tag{1}$$

where $\Omega$ is the volume of BZ and $I(V,k)$ is the $k$-resolved current. In the case of purely elastic electron flow the latter is given by the Landauer formula [41]

$$I_{\mathrm{el}}(V,k) \equiv \frac{\mathrm{G}_0}{e}\int dE\, T(E,V,k)[n_{\mathrm{F}}(E-\mu_L) - n_{\mathrm{F}}(E-\mu_R)], \tag{2}$$

where $\mathrm{G}_0 = 2e^2/h$ is the quantum of conductance, $n_{\mathrm{F}}(E)$ is the Fermi-Dirac function, and $\mu_L$ and $\mu_R$ are the chemical potentials of the left and right lead, respectively. $T(E,V,k)$ is the elastic transmission coefficient depending on energy, external bias $V$ (with $eV = \mu_L - \mu_R$), and electron momentum. In the following we will ignore bias-induced changes to it and simply write

$$T(E,k) = \mathrm{Tr}[\mathbf{G}^r \mathbf{\Gamma}_L \mathbf{G}^a \mathbf{\Gamma}_R](E,k), \tag{3}$$

where $\mathbf{G}^{r,a}(E,k)$ is the unperturbed retarded/advanced device Green's function, and $\mathbf{\Gamma}_{L/R}(E,k)$ represents the coupling to the left/right electrode.

The role of $k$-point sampling of Eqs. (1)–(3) was analyzed by Thygesen and Jacobsen [42]. They demonstrated how, for a given supercell size, a poor sampling of $k$ points in the direction transverse to transport, could lead to unphysical results. Furthermore, they pointed out that while the total energy, which depends on the integral of the DOS, is a smooth function of $k$, the transmission, which depends directly on the DOS, could present sharp features and abrupt changes as a function of $k$. In the same spirit we approach here the problem of the $k$ dependence in IETS simulations for molecular monolayers.

In presence of e-ph interactions inside the device region the current can generally be described by the Meir-Wingreen expression [43]. However, this formulation is often not practical to evaluate at the DFT-NEGF level. In the weak e-ph coupling limit a significant simplification comes from the lowest order expansion (LOE) [44–46] in which the current expression is expanded to second order in the e-ph coupling matrix $\mathbf{M}^\lambda$. We compute these couplings with finite differences of the Kohn-Sham Hamiltonian [10]. Expressed in the SIESTA basis they acquire a $k$ dependence related to the localized orbitals

$$\langle \mathbf{r}|n,k\rangle = \phi_n(r - R_n)e^{ik\cdot R_n}, \tag{4}$$

where $R_n$ is the position of orbital $n$. While the supercell approach in principle (using a sufficiently large supercell) can provide also the $q$-dependent e-ph couplings [47], we limit here to explore phonon modes commensurate with our supercells (corresponding to $q = 0$). Physically this means that we consider just vertical inelastic transitions within the electronic band structure (folded into the supercell BZ). Given the fairly localized character of the molecular vibration in the SAMs considered here, this seems a reasonable starting point for our study.

The LOE approach, recently generalized beyond the wide-band approximation to take into account the energy variation in the electronic structure on the energy scale of the phonons [48], allows us to write the current in the following $k$-resolved form

$$I^{\mathrm{LOE}}(V,k) = I_{\mathrm{el}}(V,k) + \gamma_\lambda(k)\mathcal{I}^{\mathrm{sym}}_\lambda(V) + \kappa_\lambda(k)\mathcal{I}^{\mathrm{asym}}_\lambda(V), \tag{5}$$

$$\gamma_\lambda(k) = \mathrm{Tr}[\mathbf{M}^\lambda \tilde{\mathbf{A}}_L(\mu_L)\mathbf{M}^\lambda \mathbf{A}_R(\mu_R)](k) + \mathrm{Im}B_\lambda(k), \tag{6}$$

$$\kappa_\lambda(k) = 2\mathrm{Re}B_\lambda(k), \tag{7}$$

$$B_\lambda(k) = \mathrm{Tr}[\mathbf{M}^\lambda \mathbf{A}_R(\mu_L)\mathbf{\Gamma}_L(\mu_L)\mathbf{G}^r(\mu_L)\mathbf{M}^\lambda \mathbf{A}_R(\mu_R) - \mathbf{M}^\lambda \mathbf{G}^a(\mu_R)\mathbf{\Gamma}_L(\mu_R)\mathbf{A}_R(\mu_R)\mathbf{M}^\lambda \mathbf{A}_L(\mu_L)](k), \tag{8}$$

$$\mathcal{I}^{\mathrm{sym}}_\lambda(V) = \frac{\mathrm{G}_0}{2e}\sum_{\sigma=\pm}\sigma(\hbar\omega_\lambda + \sigma eV) \times \left(\coth\frac{\hbar\omega_\lambda}{2k_BT} - \coth\frac{\hbar\omega_\lambda + \sigma eV}{2k_BT}\right), \tag{9}$$

$$\mathcal{I}^{\mathrm{asym}}_\lambda(V) = \frac{\mathrm{G}_0}{2e}\int dE[n_{\mathrm{F}}(E-eV) - n_{\mathrm{F}}(E)] \times \mathcal{H}_\epsilon\{n_{\mathrm{F}}(\epsilon - \hbar\omega_\lambda) - n_{\mathrm{F}}(\epsilon + \hbar\omega_\lambda)\}(E), \tag{10}$$

where summation over vibrational modes $\lambda$ is implicit, $\mathcal{H}_\epsilon$ is the Hilbert transform, and the partial spectral matrices $\mathbf{A}_{L,R}(E,k)$ are given by

$$\mathbf{A}_{L,R} = \mathbf{G}^r \mathbf{\Gamma}_{L,R}\mathbf{G}^a, \tag{11}$$

with time-reversed quantities $\tilde{\mathbf{A}}_{L,R} = \mathbf{G}^a \mathbf{\Gamma}_{L,R}\mathbf{G}^r$.

Finally, the IETS signal, defined as ratio between the second and first derivatives of the tunnel current $I$ with respect to the applied bias $V$, is simply sampled according to

$$\langle \mathrm{IETS}\rangle_k \equiv \frac{\sum_k d^2I(k)/dV^2}{\sum_k dI(k)/dV}. \tag{12}$$

### B. Computational details

In the present work we consider butanedithiolate (C4DT) SAMs, extending our previous study of the electrostatics and elastic transport [34], as well as a SAM of BDT between Au(111) electrodes. All four generic structures are shown in Fig. 1, namely C4DT at a tilt angle $\theta = 0^\circ$ in a dense $2\times2$ monolayer (hereafter C4DT-$2\times2-0^\circ$), C4DT at $\theta = 0^\circ$ in a dilute $4\times4$ monolayer (C4DT-$4\times4-0^\circ$), tilted C4DT at $\theta = 38^\circ$ in a dense $2\times2$ monolayer (C4DT-$2\times2-38^\circ$), and BDT in a dense $2\times2$ monolayer (BDT-$2\times2$).

Relaxation of the structures and the calculation of transmission were done using the DFT code SIESTA [49] and its transport extension TRANSIESTA [50]. We used a single-$\zeta$ plus polarization basis for gold (Au) and a double-$\zeta$ plus polarization basis for sulfur (S), hydrogen (H), and carbon (C) atoms. For gold we used the lattice constant $a = 4.18$ Å as obtained by DFT calculation. Exchange correlation was described with the generalized gradient approximation (GGA) [51]. We relaxed the molecule plus the adatom and the first gold layer until residual forces were below 0.02 eV/Å. Electronic structure was converged using a $k$-point sampling of $k = 6\times6\times1$

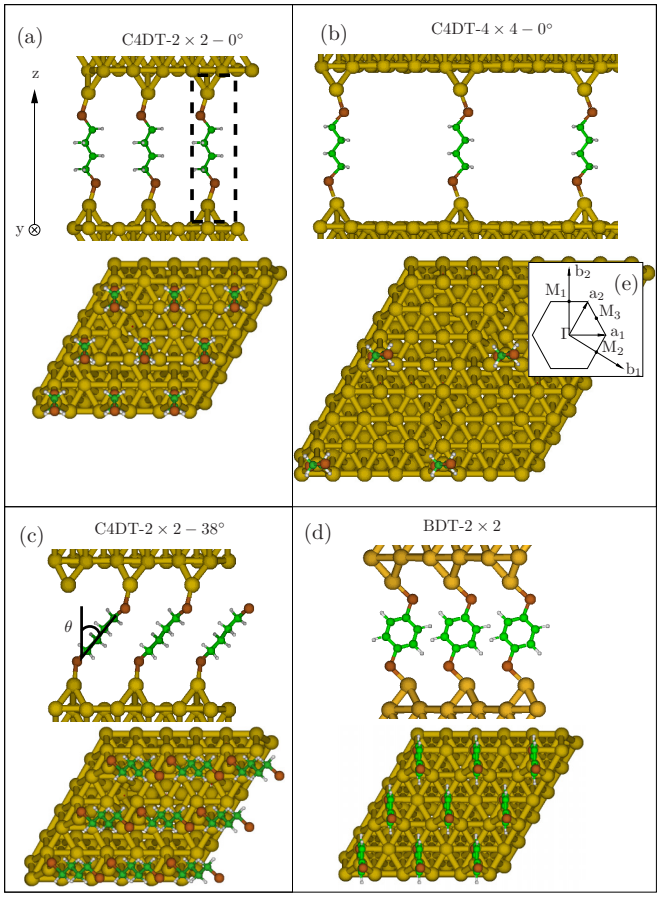


FIG. 1. (Color online) (a)–(d) Top and side view of the C4DT and BDT monolayers considered in the present work. The tilt angle $\theta$ of the alkane chain is defined as the angle between the molecular backbone and the surface normal. (e) Direct ($a_1$,$a_2$) and reciprocal ($b_1$,$b_2$) lattice vectors of the hexagonal BZ of Au(111). $M_1$, $M_2$, and $M_3$ define three symmetry points on the BZ edge.

for the dense monolayer and $k = 3 \times 3 \times 1$ for the dilute (maintaining an equivalent density of $k$ points inside the BZ for both systems).

The region enclosed by a dashed line in Fig. 1 represents the portion of the molecular junction where atoms are assumed to move. This dynamical region includes the molecule and the two adatoms. The calculations of phonon modes, e-ph couplings $\mathbf{M}^{\lambda}(k)$, and of IETS spectra were carried out with the INELASTICA package [10,52]. The e-ph coupling was calculated inside a subspace of the device region including the molecule plus the two adatoms and the first two gold layers (starting from the surface) on each side of the junction. The IETS were converged over a linear $k$-point mesh of $20 \times 20$ and $10 \times 10$ for the dense and dilute monolayers, respectively. Inversion symmetry allowed us to reduce the number of actual $k$-point evaluations by a factor of 2.

## III. RESULTS

### A. Elastic transmission

Figure 2 summarizes the electron transmission $T(E)$ (sampled over $16 \times 16$ $k$ points and $\eta = 10^{-6}$ eV for the infinitesimal imaginary part) and the projected density of states (PDOS) onto the basis orbitals of the different chemical species in the junctions (coupled to semi-infinite electrodes) of the four considered SAMs. The C4DT junctions [Figs. 2(a)–2(c)] present the characteristic band gap of an alkane chain of around 8 eV, observed in the PDOS onto H and C orbitals between $-3$ and 5 eV corresponding to the highest occupied molecular orbital (HOMO) and lowest unoccupied molecular orbital (LUMO), respectively. Transport through the C4DTs is thus characterized by electron tunneling through the tail of the HOMO level.

If we define the HOMO-LUMO gap in terms of carbon and hydrogen PDOS, we find that our BDT setup presents a smaller gap (compared to that one of C4DT) of around 5 eV, between $-2$ and 3 eV. Nevertheless, transport properties here are completely determined by a sharp sulfur-derived peak centered at the Fermi level [Fig. 2(d)] similar to previous reports with the molecule bonded via low-coordinated Au adatoms [37–39]. We note that these features may change substantially with other binding motifs [36,37,53] or by considering many-particle corrections the bare DFT-PBE spectrum [39,40]. However, for our purposes the resonant transport regime provides an interesting complementary test case qualitatively different from the other three C4DT tunnel junctions.

To understand the role of $k$ sampling in the electron transmission, Fig. 3 shows $T(E_F,k)$ at the Fermi level as a function of $k$ for the four geometries considered. In all cases a significant variation is observed over the hexagonal BZ, prompting for a careful $k$ sampling for a representative transmission probability. The local transmission minimum at the $\Gamma$ point and the features extending along the $\Gamma$-$M_1$, $\Gamma$-$M_2$, and $\Gamma$-$M_3$ directions can be traced back to the structure of the projected density of states of the electrodes (Fig. 4). The DOS of the $1 \times 1$ cell at the $\Gamma$ point is strictly zero due to the gap in the projected bands of Au(111) [54], but increasing the size of the cell ($2 \times 2$ and $4 \times 4$), band folding closes this gap in the projected bands [Figs. 4(b) and 4(c)]. Note that the hexagonal symmetry of the electrodes is lowered by each of the four SAMs. For instance, in Fig. 3(a) the $\Gamma$-$M_1$ direction is slightly different from the others. This can be explained by looking at the geometry in Fig. 1, where the molecular zigzag C-C plane introduces a given privileged direction. This effect is less evident for the diluted system in Fig. 3(b). Conversely, the symmetry breaking is rather pronounced in the cases of the tilted C4DT [Fig. 3(c)] and the BDT [Fig. 3(d)], consistent with the evident directional differences in these junctions. Clearly all these features in the $k$-resolved transmission highlight that $\Gamma$ only cannot be considered representative for the BZ average.

### B. $k$-averaged IETS

For the four geometries we compare in Fig. 5 the IETS in the commonly used $\Gamma$-point approximation, denoted IETS($\Gamma$), to the rigorously $k$-converged results, denoted $\langle \text{IETS} \rangle_k$, computed according to Eq. (12).

For the three C4DT junctions the $\Gamma$-only calculation is not a bad first approximation above $\sim$30 mV to the $k$-converged spectrum, despite the significant $k$ dependence in the elastic transmission probability discussed above. Our findings are

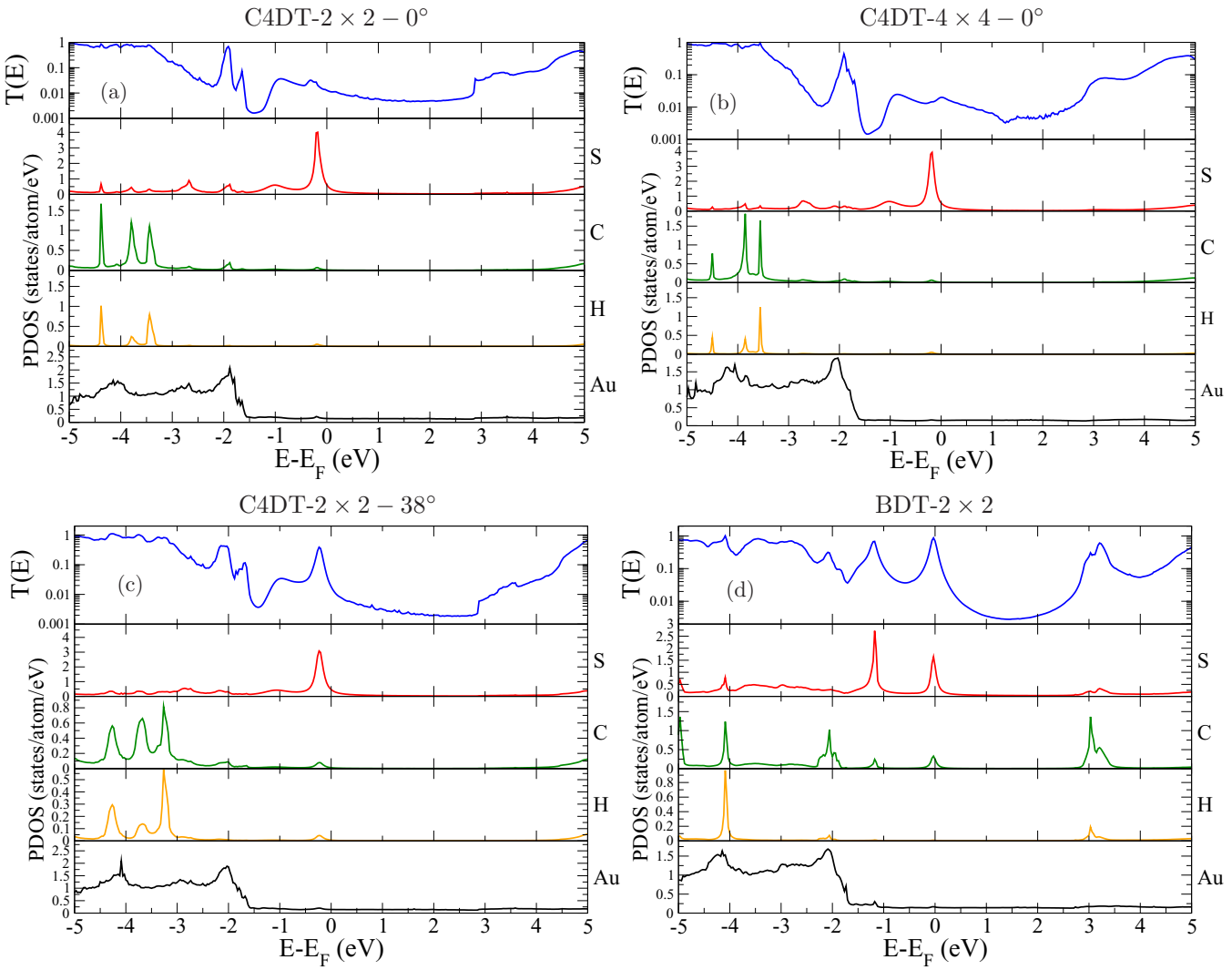


FIG. 2. (Color online) Plots of the $k$-averaged transmission function $T(E)$ and projected density of states (PDOS) over the molecular subspace in the junction for (a) C4DT-2 × 2 − 0°, (b) C4DT-4 × 4 − 0°, (c) C4DT-2 × 2 − 38°, and (d) BDT-2 × 2 − 0°.

therefore in good agreement with previous results on ADT from the literature [13,27–31]. With a broadening of $V_{\mathrm{rms}} = 5$ mV one identifies nine main peaks in the energy range above 40 meV as summarized in Table I. The high-energetic peaks are the $CH_2$ and C-C stretch modes while the low-energy peaks are associated with the heaviest sulfur and gold atoms. We also note that the C4DT spectra are almost perfectly antisymmetric with respect to bias (full lines vs dashed in Fig. 5). A detailed comparison of the IETS peak heights for the C4DT junctions reveals that the intense peaks are slightly overestimated in the Γ-only calculation, as well as some less intense peaks are underestimated.

Comparing the results for dense and dilute C4DT in Fig. 5 we see that for basically all vibrational modes the dense geometry gives a stronger signal (larger intensity) compared to the dilute. We can trace back this difference in the IETS mainly from the normalization with respect to the differential conductance, i.e., to the denominator in Eq. (12), that is about a factor of 2 larger for the dilute structure. This means that, in the dense monolayer, the fraction of incoming electrons suffering inelastic scattering processes is higher than in the dilute monolayer. Importantly, the Γ-only calculation completely misses the signal from the high-energetic CH stretch modes around 375 meV. Figure 5 also reveals that the IETS amplitudes generally increase as we introduce a tilt angle of the SAM. This effect is most pronounced for the CH stretch modes.

The situation is completely different for the BDT junction where the IETS(Γ) and $\langle \mathrm{IETS} \rangle_k$ spectra are qualitatively different. In this case $k$ averaging reduces the overall IETS signals, in particular the asymmetric contribution from $\kappa_\lambda(k)$ in Eq. (7) is observed to almost cancel out over the BZ. The differences in the voltage range below ∼30 mV are attributed to the signals corresponding to vibrations involving the heavy Au adatoms at the electrode interfaces. Based on the four different systems considered here, we note that $k$ averaging seems to have a particularly strong impact on those low-voltage signals.

### C. M(Γ) approximation

The convergence of IETS with $k$ is a computationally demanding task as e-ph coupling matrices $\mathbf{M}(k)$ and the IETS need to be computed for each $k$. For our junctions

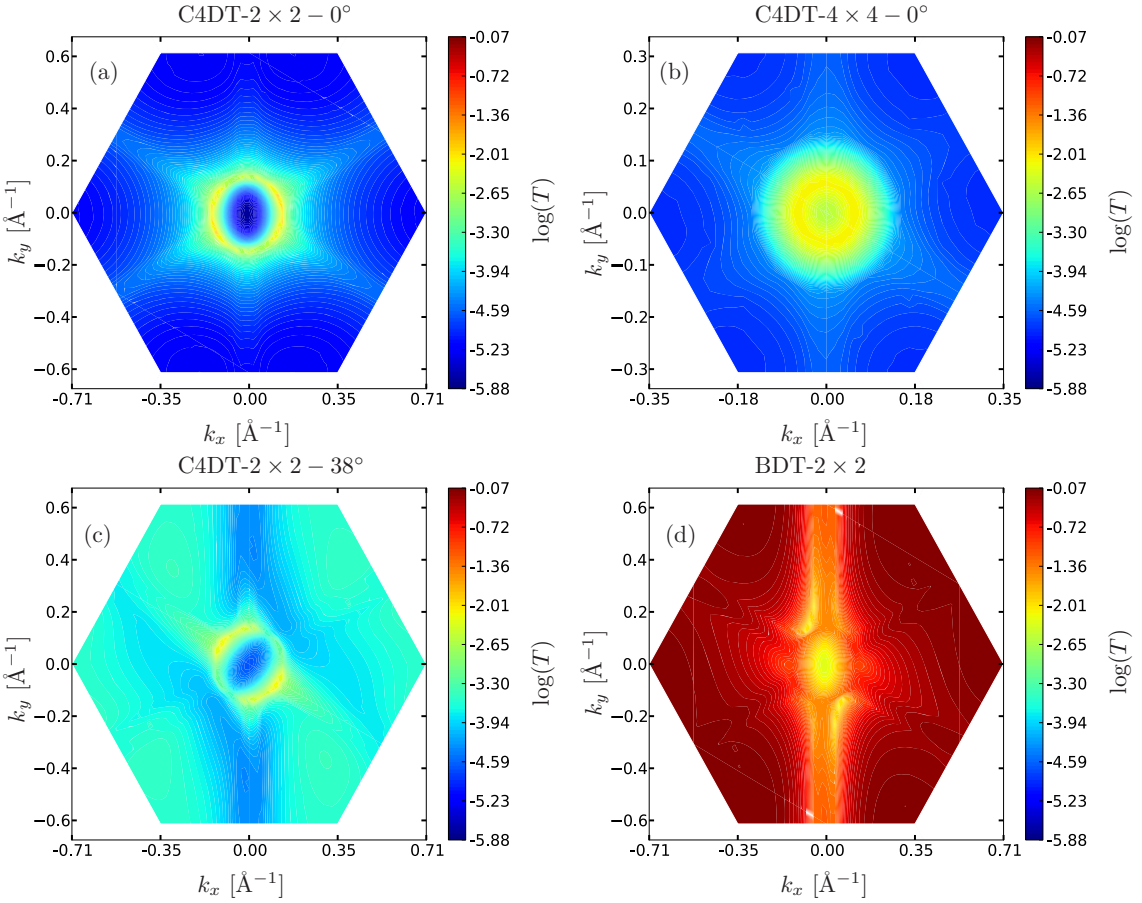


FIG. 3. (Color online) Plots of the $k$-resolved transmission at Fermi level $T(E_F,k)$ over the first BZ in the plane perpendicular to the (111) direction for: (a) C4DT-2 × 2 − 0°, (b) C4DT-4 × 4 − 0°, (c) C4DT-2 × 2 − 38°, and (d) BDT-2 × 2 − 0°. Notice the different lateral dimensions of the BZs due to varying cell sizes in real space.

we needed $20 \times 20\,k$ points for the dense monolayers and $10 \times 10\,k$ points for the dilute. However, a vast simplification is possible by choosing an appropriate definition of the phase in the basis functions. In the INELASTICA package [52] the basis functions (atomic orbitals from the SIESTA code [49]) are defined such to include a phase factor reflecting the position in different supercells. Possible phase factors associated with the intracell positions of the orbitals (e.g., as used in SIESTA) are included in the coefficients of the eigenstates.

With INELASTICA's definition, the elements of the Hamiltonian and overlap matrix can be written as

$$H_{n,m}(k) = H^0_{n,m} + \sum_{j\in \mathrm{NN}} H^j_{n,m} e^{ikR_j}, \tag{13}$$

$$S_{n,m}(k) = S^0_{n,m} + \sum_{j\in \mathrm{NN}} S^j_{n,m} e^{ikR_j}, \tag{14}$$

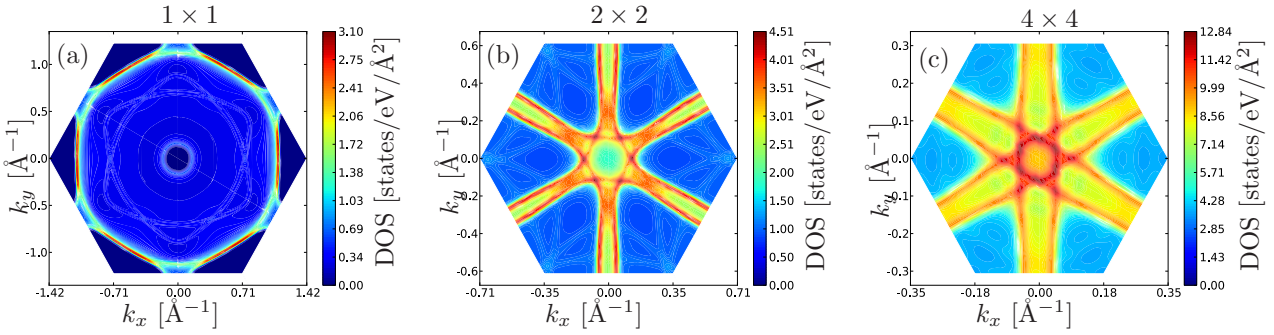


FIG. 4. (Color online) Density of states of a Au electrode at Fermi level projected on the plane perpendicular to the (111) direction using (a) (1 × 1), (b) (2 × 2), and (c) (4 × 4) supercell representations in the perpendicular plane. A sampling with 60 $k$ points along $z$ as well as a smearing of $\eta = 0.1$ eV were used.

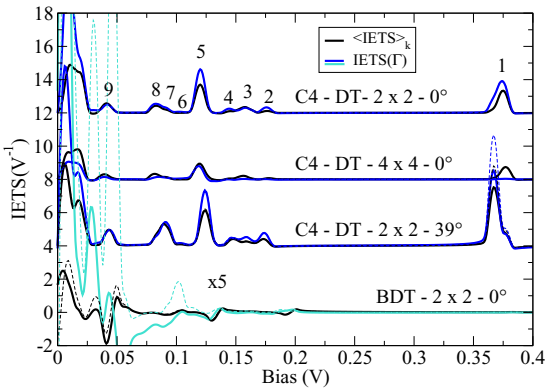


FIG. 5. (Color online) Comparison of the Γ-point approximation IETS(Γ) (blue/turquoise lines) with the $k$-converged $\langle \mathrm{IETS} \rangle_k$ (black lines) for the C4DT-2 × 2 − 0°, C4DT-4 × 4 − 0°, C4DT-2 × 2 − 38°, and the BDT-2 × 2 − 0° geometries (offset for clarity). The reverse part of the spectra for $V < 0$ is superimposed (dashed lines). The IETS of the BDT-2 × 2 − 0° geometry is multiplied by 5.

where $H^0_{n,m}$ and $S^0_{n,m}$ are the intracell Hamiltonian and overlap matrix, respectively, and the index $j$ runs over nearest neighbor (NN) supercells. The quantities $H_{n,m}(k)$ and $S_{n,m}(k)$ thus only carry a $k$ dependence due to the intercell couplings. All the intracell terms have no $k$ dependence.

If the movements of the dynamical atoms do not affect the intercell coefficients $H^j_{n,m}$ and $S^j_{n,m}$, the finite difference implementation of $\mathbf{M}(k)$ removes the $k$ dependence, and we get that also the e-ph coupling matrix does not depend on $k$. In this situation $\mathbf{M}(k) \approx \mathbf{M}(\Gamma)$ is expected to be a good approximation. Nevertheless, in general, since the electronic structure and the elastic transport properties depend on $k$ when intercell couplings are present [through Eqs. (13) and (14)], a proper $k$ sampling of the IETS is still required. The $\mathbf{M}(\Gamma)$ approximation just implies that one can reuse the e-ph couplings computed at one *single* $k$ point for all other points in the $k$ mesh for the IETS.

The $\mathbf{M}(\Gamma)$ approximation is validated in Fig. 6 for our molecular junctions. For the vertical geometries ($\theta = 0°$) it

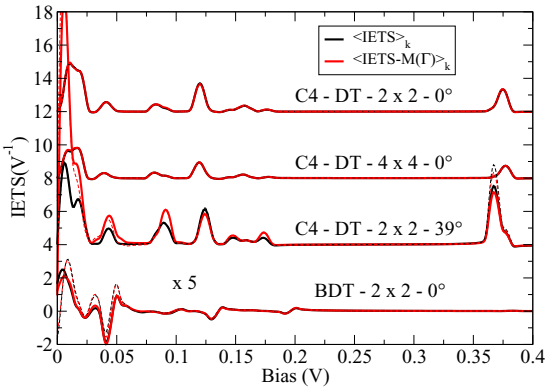


FIG. 6. (Color online) Comparison of $k$-averaged IETS with the $\mathbf{M}(\Gamma)$ approximation (red lines) with the full $\langle \mathrm{IETS} \rangle_k$ calculation (black lines) for the C4DT-2 × 2 − 0°, C4DT-4 × 4 − 0°, C4DT-2 × 2 − 38°, and the BDT-2 × 2 − 0° geometries. The reverse part of all spectra for $V < 0$ is superimposed (dashed lines). The IETS of the BDT-2 × 2 − 0° geometry is multiplied by 5.

TABLE I. List of main inelastic peaks in the IETS and description of the corresponding vibrational modes for the C4DT-2 × 2 − 0° geometry reported in Fig. 5.

| Peak number | Number of modes | Energy (meV) | Description |
|---|---|---|---|
| 1 | 8 | 367–378 | $CH_2$ stretch |
| 2 | 4 | 175–178 | $CH_2$ scissor |
| 3 | 4 | 155–160 | $CH_2$ wag + twist |
| 4 | 3 | 138–145 | $CH_2$ wag + twist + rock + S-C stretch + C-C stretch |
| 5 | 5 | 116–126 | C-C stretch |
| 6 | 1 | 102 | $CH_2$ rock |
| 7 | 2 | 87–90 | $CH_2$ rock |
| 8 | 2 | 81 | S-C stretch |
| 9 | 4 | 39–48 | S-adatom stretch + C-S-adatom scissor |

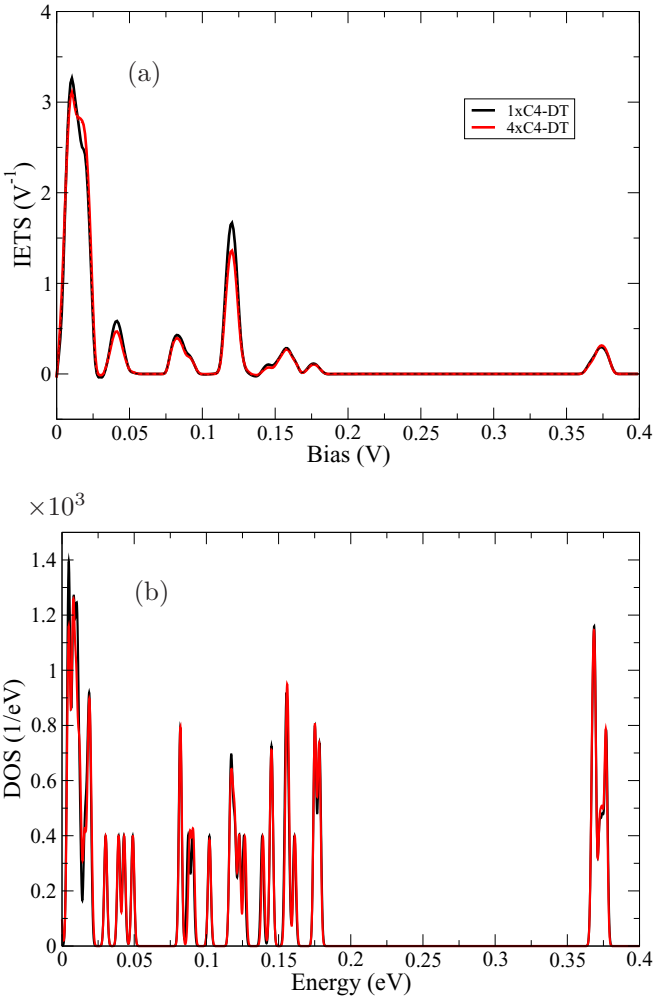


FIG. 7. (Color online) Comparison of (a) IETS in the $\mathbf{M}(\Gamma)$ approximation and (b) vibrational density of states for the C4DT-2 × 2 − 0° structure in two different cell sizes normalized with respect to the number of supercells; a small Gaussian broadening of 1 meV is used.

is very accurate while some deviation is observed for the tilted geometry. To exclude that these deviations are not simply due to phase cancellations in the summation over cells for the most symmetric geometries, we performed a check with tilted C4DT in a dilute configuration only to find essentially identical IETS for $k$-sampled and $\Gamma$-only treatments. Hence, this supports that the accuracy of $\Gamma$ only is mainly limited by the magnitude of the intermolecular couplings.

### D. Investigation of the $q = 0$ approximation

Finally, in order to explore the $q = 0$ approximation for the phonons we also calculated the IETS for the dense C4DT-$2 \times 2 - 0^\circ$ structure in a $4 \times 4$ supercell representation. This larger cell thus contains four molecules (denoted $4 \times$ C4DT to distinguish it from the representation $1 \times$ C4DT with a single molecule in the small cell). As the dynamical region now contains four molecules and the respective adatoms, the phonon band folding gives four times the number of modes at the $\Gamma$ point of the large cell. Consequently, a $\Gamma$-point calculation in the large cell will account for many more inelastic processes.

We fixed the geometry C4DT-$2 \times 2 - 0^\circ$ obtained from relaxations with the small cell and simply duplicated out in the directions perpendicular to the transport. The charge density was converged with an equivalent $k$-point density in BZ. Figure 7(a) shows the $k$-converged IETS in the $\mathbf{M}(\Gamma)$ approximation for the $1 \times$ C4DT and the $4 \times$ C4DT geometries. Interestingly, this comparison also supports the validity of the $q = 0$ approximation for ADT monolayers, even in the dense configuration.

In Fig. 7(b) are plotted the vibrational density of states in the two cases. As we can see folding the phonon band structure does not introduce additional features in the DOS. This reflects the mostly negligible dispersion of the intramolecular modes of the monolayer with $q$. This explain why the IETS of the $1 \times$ C4DT and the $4 \times$ C4DT geometries present the same peaks.

## IV. CONCLUSIONS

We have calculated the IETS of molecular monolayers formed by ADT and BDT using a periodic DFT supercell approach in the plane perpendicular to the transport. We considered high ($2 \times 2$) and low ($4 \times 4$) coverage conditions and two different tilt angles. We presented a comparison between the commonly used $\Gamma$-point calculation (for both electrons and phonons) with a more rigorous $k$-averaged result. Although for ADT the $\Gamma$-point calculation reproduces the overall features of the $k$-averaged IETS (apart a certain deviation in the peak amplitudes), for BDT the two calculations differ substantially. Thus, in general, the correct IETS intensity of the active modes relies on proper $k$-point sampling. In order to reduce the computational cost of IETS calculation we propose an approximation method where the $k$-averaged IETS is evaluated at each $k$ using the $\Gamma$-point e-ph coupling matrix. This approximation provides an accurate result in all those cases where the dynamical atoms do not modify the intercell coupling terms in the Hamiltonian. Finally, we also investigated the $q = 0$ approximation for the phonons by doubling the supercell in real space.

## ACKNOWLEDGMENTS

We acknowledge the support of the Basque Departamento de Educación and the UPV/EHU (Grant No. IT-756-13), the Spanish Ministerio de Economía y Competitividad (MINECO Grants No. MAT2013-46593-C6-2-P and FIS2013-48286-C2-2-P), and the European Union Integrated Project PAMS (Contract No. 610446).

[1] K. W. Hipps and U. Mazur, Inelastic electron tunneling: An alternative molecular spectroscopy, J. Phys. Chem. **97**, 7803 (1993).

[2] M. Galperin, M. A. Ratner, and A. Nitzan, Molecular transport junctions: Vibrational effects, J. Phys.: Condens. Matter **19**, 103201 (2007).

[3] M. A. Reed, Inelastic electron tunneling spectroscopy, Mater. Today **11**, 46 (2008).

[4] T. Frederiksen, M. Brandbyge, N. Lorente, and A.-P. Jauho, Inelastic scattering and local heating in atomic gold wires, Phys. Rev. Lett. **93**, 256601 (2004).

[5] A. Pecchia, A. Di Carlo, A. Gagliardi, S. Sanna, T. Frauenheim, and R. Gutierrez, Incoherent electron-phonon scattering in octanethiols, Nano Lett. **4**, 2109 (2004).

[6] A. Troisi and M. A. Ratner, Modeling the inelastic electron tunneling spectra of molecular wire junctions, Phys. Rev. B **72**, 033408 (2005).

[7] J. Jiang, M. Kula, W. Lu, and Y. Luo, First-principles simulations of inelastic electron tunneling spectroscopy of molecular electronic devices, Nano Lett. **5**, 1551 (2005).

[8] N. Sergueev, D. Roubtsov, and H. Guo, *Ab initio* analysis of electron-phonon coupling in molecular devices, Phys. Rev. Lett. **95**, 146803 (2005).

[9] G. C. Solomon, A. Gagliardi, A. Pecchia, T. Frauenheim, A. Di Carlo, J. R. Reimers, and N. S. Hush, Understanding the inelastic electron-tunneling spectra of alkanedithiols on gold, J. Chem. Phys. **124**, 094704 (2006).

[10] T. Frederiksen, M. Paulsson, M. Brandbyge, and A.-P. Jauho, Inelastic transport theory from first principles: Methodology and application to nanoscale devices, Phys. Rev. B **75**, 205413 (2007).

[11] H. Nakamura, K. Yamashita, A. R. Rocha, and S. Sanvito, Efficient *ab initio* method for inelastic transport in nanoscale devices: Analysis of inelastic electron tunneling spectroscopy, Phys. Rev. B **78**, 235420 (2008).

[12] A. Garcia-Lekue, D. Sanchez-Portal, A. Arnau, and T. Frederiksen, Simulation of inelastic electron tunneling spectroscopy of single molecules with functionalized tips, Phys. Rev. B **83**, 155417 (2011).

[13] Y. Kim, T. J. Hellmuth, M. Bürkle, F. Pauly, and E. Scheer, Characteristics of amine-ended and thiolended alkane single-molecule junctions revealed by inelastic electron tunneling spectroscopy, ACS Nano **5**, 4104 (2011).

[14] E. T. R. Rossen, C. F. J. Flipse, and J. I. Cerdá, Lowest order in inelastic tunneling approximation: Efficient scheme for

simulation of inelastic electron tunneling data, Phys. Rev. B **87**, 235412 (2013).

[15] Here we consider periodic systems in the plane ($x$-$y$) transverse to the transport direction ($z$) and therefore always refer to parallel electron and phonon momenta.

[16] X. D. Cui, A. Primak, X. Zarate, J. Tomfohr, O. F. Sankey, A. L. Moore, T. A. Moore, D. Gust, G. Harris, and S. M. Lindsay, Reproducible measurement of single-molecule conductivity, Science **294**, 571 (2001).

[17] X. Li, J. He, J. Hihath, B. Xu, S. M. Lindsay, and N. Tao, Conductance of single alkanedithiols: Conduction mechanism and effect of molecule-electrode contacts, J. Am. Chem. Soc. **128**, 2135 (2006).

[18] C. Li, I. Pobelov, T. Wandlowski, A. Bagrets, A. Arnold, and F. Evers, Charge transport in single au—alkanedithiol—au junctions: Coordination geometries and conformational degrees of freedom, J. Am. Chem. Soc. **130**, 318 (2008).

[19] Y. Li, Z. Yin, J. Yao, and J. Zhao, First-principles study of the electron transport of single alkanedithiol molecule under the influence of compression, Chem. Lett. **38**, 334 (2009).

[20] M. Paulsson, C. Krag, T. Frederiksen, and M. Brandbyge, Conductance of alkanedithiol single-molecule junctions: A molecular dynamics study, Nano Lett. **9**, 117 (2009).

[21] W. Wang, T. Lee, I. Kretzschmar, and M. A. Reed, Inelastic electron tunneling spectroscopy of an alkanedithiol self-assembled monolayer, Nano Lett. **4**, 643 (2004).

[22] J. G. Kushmerick, J. Lazorcik, C. H. Patterson, R. Shashidhar, D. S. Seferos, and G. C. Bazan, Vibronic contributions to charge transport across molecular junctions, Nano Lett. **4**, 639 (2004).

[23] M. Paulsson, T. Frederiksen, and M. Brandbyge, Inelastic transport through molecules: Comparing first-principles calculations to experiments, Nano Lett. **6**, 258 (2006).

[24] D. P. Long, J. L. Lazorcik, B. A. Mantooth, M. H. Moore, M. A. Ratner, A. Troisi, Y. Yao, J. W. Ciszek, J. M. Tour, and R. Shashidhar, Effects of hydration on molecular junction transport, Nat. Mater. **5**, 901 (2006).

[25] J. M. Beebe, H. J. Moore, T. R. Lee, and J. G. Kushmerick, Vibronic coupling in semifluorinated alkanethiol junctions: Implications for selection rules in inelastic electron tunneling spectroscopy, Nano Lett. **7**, 1364 (2007).

[26] H. Song, Y. Kim, Y. H. Jang, H. Jeong, M. A. Reed, and T. Lee, Observation of molecular orbital gating, Nature (London) **462**, 1039 (2009).

[27] N. Okabayashi, Y. Konda, and T. Komeda, Inelastic electron tunneling spectroscopy of an alkanethiol self-assembled monolayer using scanning tunneling microscopy, Phys. Rev. Lett. **100**, 217801 (2008).

[28] N. Okabayashi, M. Paulsson, H. Ueba, Y. Konda, and T. Komeda, Site selective inelastic electron tunneling spectroscopy probed by isotope labeling, Nano Lett. **10**, 2950 (2010).

[29] N. Okabayashi, M. Paulsson, H. Ueba, Y. Konda, and T. Komeda, Inelastic tunneling spectroscopy of alkanethiol molecules: High-resolution spectroscopy and theoretical simulations, Phys. Rev. Lett. **104**, 077801 (2010).

[30] C. R. Arroyo, T. Frederiksen, G. Rubio-Bollinger, M. Vélez, A. Arnau, D. Sánchez-Portal, and N. Agräit, Characterization of single-molecule pentanedithiol junctions by inelastic electron tunneling spectroscopy and first-principles calculations, Phys. Rev. B **81**, 075405 (2010).

[31] Y. Kim, H. Song, F. Strigl, H.-F. Pernau, T. Lee, and E. Scheer, Conductance and vibrational states of single-molecule junctions controlled by mechanical stretching and material variation, Phys. Rev. Lett. **106**, 196804 (2011).

[32] J.-G. Wang, E. Prodan, R. Car, and A. Selloni, Band alignment in molecular devices: Influence of anchoring group and metal work function, Phys. Rev. B **77**, 245443 (2008).

[33] T. Frederiksen, C. Munuera, C. Ocal, M. Brandbyge, M. Paulsson, D. Sánchez-Portal, and A. Arnau, Exploring the tilt-angle dependence of electron tunneling across molecular junctions of self-assembled alkanethiols, ACS Nano **3**, 2073 (2009).

[34] G. Foti, D. Sánchez-Portal, A. Arnau, and T. Frederiksen, Interface dipole effects as a function of molecular tilt: Mechanical gating of electron tunneling through self-assembled monolayers? J. Phys. Chem. C **117**, 14272 (2013).

[35] M. A. Reed, C. Zhou, C. J. Muller, T. P. Burgin, and J. M. Tour, Conductance of a molecular junction, Science **278**, 252 (1997).

[36] E. G. Emberly and G. Kirczenow, The smallest molecular switch, Phys. Rev. Lett. **91**, 188301 (2003).

[37] J. Tomfohr and O. F. Sankey, Theoretical analysis of electron transport through organic molecules, J. Chem. Phys. **120**, 1542 (2004).

[38] D. J. Mowbray, G. Jones, and K. S. Thygesen, Influence of functional groups on charge transport in molecular junctions, J. Chem. Phys. **128**, 111103 (2008).

[39] V. M. García-Suárez and C. J. Lambert, First-principles scheme for spectral adjustment in nanoscale transport, New J. Phys. **13**, 053026 (2011).

[40] M. Strange, C. Rostgaard, H. Hakkinen, and K. S. Thygesen, Self-consistent GW calculations of electronic transport in thiol- and amine-linked molecular junctions, Phys. Rev. B **83**, 115108 (2011).

[41] R. Landauer, Spatial variation of currents and fields due to localized scatterers in metallic conduction, IBM J. Res. Dev. **1**, 223 (1957).

[42] K. S. Thygesen and K. W. Jacobsen, Interference and $k$-point sampling in the supercell approach to phase-coherent transport, Phys. Rev. B **72**, 033401 (2005).

[43] Y. Meir and N. S. Wingreen, Landauer formula for the current through an interacting electron region, Phys. Rev. Lett. **68**, 2512 (1992).

[44] M. Paulsson, T. Frederiksen, and M. Brandbyge, Modeling inelastic phonon scattering in atomic- and molecular-wire junctions, Phys. Rev. B **72**, 201101 (2005).

[45] J. K. Viljas, J. C. Cuevas, F. Pauly, and M. Häfner, Electron-vibration interaction in transport through atomic gold wires, Phys. Rev. B **72**, 245415 (2005).

[46] F. Haupt, T. Novotný, and W. Belzig, Current noise in molecular junctions: Effects of the electron-phonon interaction, Phys. Rev. B **82**, 165441 (2010).

[47] K. Kaasbjerg, K. S. Thygesen, and K. W. Jacobsen, Phonon-limited mobility in n-type single-layer $MoS_2$ from first principles, Phys. Rev. B **85**, 115317 (2012).

[48] J.-T. Lü, R. B. Christensen, G. Foti, T. Frederiksen, T. Gunst, and M. Brandbyge, Efficient calculation of inelastic vibration signals in electron transport: Beyond the wide-band approximation, Phys. Rev. B **89**, 081405 (2014).

[49] J. M. Soler, E. Artacho, J. D. Gale, A. Garca, J. Junquera, P. Ordejn, and D. Sánchez-Portal, The siesta method for *ab initio*

order- n materials simulation, J. Phys.: Condens. Matter **14**, 2745 (2002).

[50] M. Brandbyge, J.-L. Mozos, P. Ordejón, J. Taylor, and K. Stokbro, Density-functional method for nonequilibrium electron transport, Phys. Rev. B **65**, 165401 (2002).

[51] J. P. Perdew, K. Burke, and M. Ernzerhof, Generalized gradient approximation made simple, Phys. Rev. Lett. **77**, 3865 (1996).

[52] INELASTICA is freely available at http://sourceforge.net/projects/inelastica

[53] F. Evers, F. Weigend, and M. Koentopp, Conductance of molecular wires and transport calculations based on density-functional theory, Phys. Rev. B **69**, 235411 (2004).

[54] S. D. Kevan and R. H. Gaylord, High-resolution photoemission study of the electronic structure of the noble-metal (111) surfaces, Phys. Rev. B **36**, 5809 (1987).